RESEARCH
www.commprac.com
ISSN 1462 2815

OPTIMIZATION AND FORMULATION OF ERIBULIN BASED SILVER NANOPARTICLES LOADED MICROEMULSION FOR TARGETED ORAL DELIVERY SYSTEM: A COST-EFFECTIVE AND ECO-FRIENDLY APPROACH WITH DUAL ANTICANCER AND ANTIBACTERIAL PROPERTIES

Jiyaul Hak [1]*, Dinesh Kumar Sharma [2], Nasiruddin Ahmad Farooqui [3] and Iram Jahan [4]

[1] Research Scholar, Sanskriti University, Mathura-Delhi Highway, Chhata, Mathura, U.P., India. *Corresponding Author Email: jiyaultiper@gmail.com
[2] Professor, Sanskriti University, Mathura-Delhi Highway, Chhata, Mathura, U.P., India
[3] Professor, Translam Institute of Pharmaceutical Education and Research, Meerut, U.P., India.
[4] Assistant Professor, IIMT College of Medical Sciences, IIMT University, O-Pocket, Ganganagar, Meerut, U.P., India.

DOI: 10.5281/zenodo.10663865

Abstract

The most frequent sickness to affect women is breast cancer. A targeted drug delivery strategy for an anticancer agent is required to treat breast cancer (BC) cells to the appropriate therapeutic potential without endangering healthy cells. The main objective of this work is to optimise and synthesise silver nanoparticles (AgNPs) for oral usage in a cost-effective and ecologically friendly way. Furthermore, using animal models and cancer cell lines, AgNPs laden ME will be examined for antibacterial and anticancer properties. Eribulin is a synthetic medication having potent anticancer effects against breast cancer. A neural network (NN) optimisation technique was used to synthesise AgNPs and determine the relationship between the formulation elements and response variables (AgNPs size). For the improved AgNPs in the AgNPs loaded ME formulation, evaluations were conducted regarding particle size and shape, morphological characterisation, particle charge, and in vitro drug release investigations. The 3-factor, D-optimal mixture model and the pseudo-ternary phase diagram were used for the synthesis and evaluation of AgNPs loaded ME. The microemulsion containing silver nanoparticles was evaluated for its physicochemical properties, particle size, shape, surface morphology, zeta potential and in vitro release assays. AgNPs loaded ME exhibit active drug release, which increases the drug's therapeutic concentration and bioavailability in cancer cells compared to healthy cells. In addition to having great anticancer potential against MCF-7 cancer cells, the synthetic AgNPs in the AgNPs-loaded microemulsion may also be able to stop the growth of bacteria. The in-vivo study revealed that, in comparison to the tumor control, swallowing AgNPs-loaded ME formulations dramatically decreased the tumor mass and Ehrlich ascites solid tumor development rate in the mice. The results indicate that AgNPs in AgNPs loaded ME appear promising as an anticancer therapy in terms of stability, cost, and simplicity of fabrication.

Keywords: Silver Nanoparticles Loaded Microemulsion, breast cancer, Anticancer and Antibacterial Properties, Eribulin.

1. INTRODUCTION

Nanotechnology has emerged as a revolutionary field with the potential to transform various industries, ranging from medicine to electronics. Among the diverse applications of nanomaterials, silver nanoparticles (AgNPs) have garnered significant attention due to their unique properties and versatile applications. In recent years, the integration of AgNPs into various delivery systems has become a focal point of research, aiming to enhance their stability, bioavailability, and efficacy in different applications [1]. Microemulsions, as a colloidal system, have gained prominence as efficient carriers for the delivery of active compounds, owing to their ability to solubilize hydrophobic and hydrophilic components simultaneously. The incorporation of AgNPs

into microemulsions represents a promising avenue for overcoming challenges associated with AgNPs, such as agglomeration and limited stability in aqueous environments. This synergistic combination offers a platform for controlled and targeted delivery of AgNPs, unlocking new possibilities in diverse fields, including medicine, agriculture, and environmental science [2].

This introduction chapter provides a comprehensive overview of the key elements that form the basis of AgNPs loaded microemulsion research. It begins by elucidating the distinctive properties of AgNPs, emphasizing their antimicrobial, catalytic, and optical characteristics. Subsequently, the focus shifts to microemulsions, exploring their structure, formulation, and advantages as carriers for active ingredients. The rationale behind the integration of AgNPs into microemulsions is then discussed, highlighting the potential benefits and addressing challenges associated with this novel hybrid system [3]. The rest of this document will delve into the current state of research in the field, discussing relevant studies and advancements. Furthermore, it will outline the objectives and significance of the present study, shedding light on the potential contributions to the existing body of knowledge. As the exploration of AgNPs loaded microemulsions continues to unfold, the subsequent chapters will provide a detailed examination of the methodologies, results, and implications, contributing to the ever-expanding landscape of nanotechnology and colloid science [4]. AgNPs were produced in this work using the non-toxic reducing agent Eribulin microemulsion method. The qualities of the breast cancer therapy approved by medicine dictate which reducing agent is utilised. In the microemulsion procedure, we have used a non-toxic solvent and a surfactant. The experimental setup will be modified using variables to maximise the production of silver nanoparticles. Eribulin will be utilised to study the antibacterial and anticancer effects of AgNPs laden ME, which were produced in vivo and in vitro by a reduction process. The next paragraphs provide an explanation of the research methodology, therapeutic use, and characterization of AgNPs. AgNP synthesis within a ME filled with AgNP [5].

2. MATERIAL AND METHODS

2.1 Synthesis of AgNPs loaded Microemulsion

The pseudo-ternary phase diagram, which showed the makeup of the w/o microemulsion production region, was created using the aqueous burette titration method. The combination compositions of oil, surfactant, and water for creating microemulsion were determined by looking at the produced ternary phase diagram [6].

2.2 Construction of ternary phase diagrams for *w/o* microemulsion

Using the aqueous titration approach, the pseudo-ternary phase diagram of the ME was created (Neeraj Kumar & Shishu, 2015b)(Ke, Lin, Ho, & Sheu, 2005). For the purpose of creating phase diagrams, oil (IPM) and surfactant (AOT) were combined in test tubes at different %w/w ratios, ranging from 1:9 to 9:1, and mixed using a vibromixer at room temperature (25°C) (Neeraj Kumar & Shishu, 2015b). After that, the oil and surfactant mixtures were individually treated to the addition of AgNO3 and the Eribulin solution, allowing the microemulsion synthesis area to be seen on the phase diagram. For a full day to allow for equilibration, all microemulsion systems were maintained at a consistent temperature of 25±2°C. Eribulin optical clarity and fluidity were tracked throughout this time [7].

2.3 Synthesis of AgNPs loaded *w/o* microemulsion

For both varieties of the microemulsion, W_{AOT}, or the mass ratio of AOT to the total mass of AOT and IPM mixture[AOT]/[AOT+IPM], was set at 0.3. To create w/o microemulsions, the concentration of AgNO3 and Eribulin were added as the silver precursor and a reductant was maintained at 0.1 and 0.3 mm, respectively. The ternary phase diagram was used to determine the combination compositions of oil, surfactant, and water for creating microemulsion. The synthesis of AgNPs involved the gradual blending of microemulsions A, which contained AgNO3 solution, and B, which contained Eribulin solution with the same water to surfactant ratio (w), drop by drop for one hour. The mixture was then agitated for three hours at a magnetic stirrer (Feng et al., 2013b). AgNP production is indicated by the progressive development of a yellow to dark brown colour with the addition of Eribulin microemulsion to silver precursor microemulsion (Singha, Barman, & Sahu, 2014b). Using a magnetic stirrer set to 300 rpm and 25±2°C, vigorous stirring was maintained during the entire mixing phase. AgNP production in ME was recorded using a UV-visible spectrophotometer. Figure 5.2 showed a diagrammatic illustration of the synthesis of AgNPs in an AOT microemulsion [8]. The phase diagram's microemulsion synthesis area was identified by the addition of AgNO3 and the Eribulin solution, respectively, to the oil and surfactant combination. For a whole day, all microemulsion systems were allowed to acclimatise to a room temperature of 25°C. Throughout this time, the phase changes in terms of visual clarity and fluidity were noted [9].

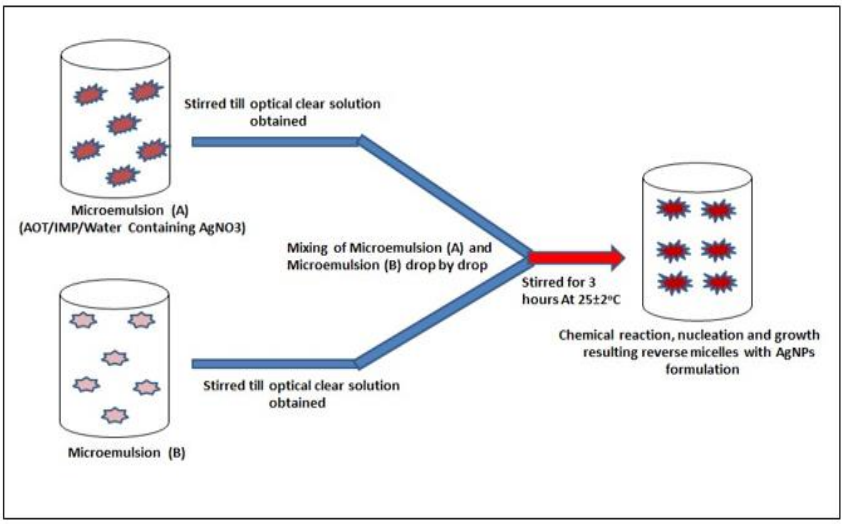

Figure 1: Diagrammatic representation of AgNPs synthesis using water-in-oilmicroemulsion

2.4 Optimization model (D-optimal Mixture Design)

Using a three-component mixture experimental design of D-optimal, the effects of formulation variables, namely, %w/w of IPM (A), AOT (B), and silver precursor or reducing agent (AgNO3: Eribulin) (C), on particle size, viscosity, pH, and % drug release, were investigated. When creating the D-optimal mixed model, independent variables (Xi) are subject to certain lower (Li) and higher (Ui) limits for the synthesis of ME [10]. Mixture limits can be expressed using the following equation:

$$\Sigma iXi = 1 \; and \; Li \leq Xi \leq Ui$$

In optimal mixture model, output variable(*Y*) optimization depends on the actualvalues of the input factors, *Xi*.

$$Y = (X_1, X_2, X_3, X_4 \ldots X_n)$$

2.5 Statistical Analysis

The statistical software Design Expert®, version 10.0, USA, was used for the statistical analysis. A substantial p-value ($p<0.05$) and an R2 value more than 0.9, which denotes a strong correlation in the model, are both necessary for an optimised model to be effective [11].

2.6 Verification of model

Twelve random formulations were made using Design Expert, and the constructed model was validated by statistically comparing the actual and model predicted values. Using residual standard error (RSE), the following calculation (Samson et al., 2016a) was used to compare the model anticipated outcomes with actual results:

$$\boldsymbol{RSE}\ \% = \frac{\boldsymbol{Experimental\ value - Predicted\ value}}{\boldsymbol{Predicted\ value}} \times \mathbf{100}$$

3. CHARACTERIZATION TECHNIQUES OF OPTIMIZED AgNPS LOADED ME

3.1 UV-visible absorption spectral analysis: UV-visible spectrometer was employed to document the AgNP-loaded microemulsion's production. A 10 mm cuvette was utilized to record the absorption spectra using a Perkin-Elmer Lambda-760 spectrophotometer. Spectra in the 200–800 nm regions were recorded to track the AgNP synthesis in w/o ME [12].

3.2 Particle Size and dispersity Index (PDI): DLS technique is used for determining particle size and PDI of the AgNPs using nano-Zetasizer, dispersed at an angle of 90o at an ambient condition of 25oC. This technique used primarily for measuring the Brownian motion of particles in the nano and micron range and their uniformity in colloidal suspensions. PDI determines the uniform dispersion of particles [13].

3.3 Transmission electron microscopy (TEM): Using the Jeol TEM 1011, the morphological form, size, and structure of the AgNPs loaded microemulsion were examined. The formulation sample was put on copper-coated grids after being sonicated for five minutes to ensure a homogeneous dispersion of nanoparticles. It was then allowed to air dry at room temperature, namely 25±0.50C [14].

3.4 Viscosity, pH and Conductivity: AgNPs loaded ME at 250C were viscosity measured using spindle no. 62 of the Brookfield Pro viscometer of LVDV-II+ (Middleboro, MA, USA). The pH of the AgNP-filled microemulsion was measured using a pH meter. After calibrating the pH meter, measurements were made. A conductivity meter was used to test the microemulsion's conductivity at an ambient temperature of 25±50C. The conductivity meter uses a platinum conductance electrode with an operating frequency of 50 Hz and a cell constant value of k=1. For determining the phase inversion process and confirming the kind of microemulsion, it is an essential feature. The nature or structure of the microemulsion is determined by the percolation process.

3.5 Density: The AgNPs loaded ME density was determined using a glass Pycnometer. Before starting the experiment, the empty weight of the pycnometer is

measured. The weight of a pycnometer that had been filled to the neck with pure water was then measured using a calibrated electronic measuring balance. The density of distilled water is then calculated using the volume of distilled water that was measured in the pycnometer. Subsequently, the produced ME preparation density loaded with synthesized AgNPs was calculated using an analogous procedure. The following equation represents the density formula:

$$Density\ \left(\frac{g}{ml}\right) = \frac{Mass\ (g)}{Volume\ (ml)}$$

3.6 Surface tension measurement: The stability of ME is determined by the surface tension of the microemulsion. In order to increase the surface area and cause the dispersion of water or oil droplets (micro-emulsification), a low surface tension value necessitates low energy and a physically stable ME system. Using a CSC scientific Tensiometer (Akem pharmaceuticals & Pharmamaceutical Ltd., Haridwar, Uttarakhand), the surface tension film of the optimised AgNPs loaded ME was measured at 25±0.50C. The test sample's surface tension was measured using a DuNouy ring-type tensiometer. Using this approach, the test sample is put in a platinum ring to achieve equilibrium conditions at room temperature, 25±0.50C. The platinum ring's surface tension, measured in dynes/centimeter, is the force that breaks the surface.

3.7 Zeta potential determination: The surface charge of the particles was measured at 25±0.50C using the nano-Zetasizer (Malvern Instrument Ltd., UK). The electrophoretic motions of scattering particles in a charged field were used to calculate the zeta potential. Zeta cells with modest volumes that were disposable were used for the measurements. Zeta potential measurements were performed after samples were sonicated for ten minutes.

3.8 Fourier transform infrared (FTIR) analysis: IR study of the AgNPs loaded microemulsion was applied to determine the primary functional groups of the compounds which are responsible for AgNPs synthesis in ME andpossible interactions between excipients. FTIR measurements were carried out using a Shimadzu 8400S spectrophotometer by employing the KBr disc technique. The FTIR spectrum of the formulation was recorded at a resolution of 4 cm^{-1} in the transmission mode (4000–440cm^{-1}).

3.9 Refractive Index (RI): The refractive index measurement was used to determine the isotropic optical nature of ME using the instrument Abbe refractometer (ELICO, India) which contains a pair of glass prisms in between liquid film was placed. The RI was determined by keepinga drop of test sample on the glass slide using a syringe, and reading was recorded on a measuring scale using a polarizing microscope under the effect of polarized light. Then thescale of the refractometer was adjusted using micrometric screw in such a way that clear interface between the illuminated and dark regions could be observed and finally record the RI value from a scale [15].

3.10 Rheological behavior measurements: The rheometer (LVDV- III Ultra) was used to examine the flow behaviour of AgNPs loaded ME. The temperature of 25.0±0.20C was employed, and the shear rate was measured between 10^{-3} and 10^{5} s^{-1} (n=3). Structural behaviour is determined by rheology behaviour, which also provides stability information for ME systems.

3.11 Drug content of Eribulin: ME loaded with AgNPs (0.10 g) was dissolved in 10 ml of ethanol by sonication for five minutes, allowing for complete dissolution of ME. The sample was then measured spectrophotometrically at 280 nm [16]. Next, the formula determines the proportion of drug content.

3.11 Inductively coupled plasma mass spectrometry (ICP-MS) analysis: This analytical technique determines the metal content and relative efficiency for AgNPs loaded ME using an Agilent 7900 ICP-MS. It was used to ascertain the formulations' silver (Ag) content in a time dependent manner. The calibration curve was prepared and analyzed using AgNO3 as a blank solution. The dialysis bag method was used in this instance. Next, the time-dependent Ag ion release mechanism was evaluated in the filtered solution.

3.11 Inductively coupled plasma mass spectrometry (ICP-MS) analysis: This analytical technique determines the metal content and relative efficiency for AgNPs loaded ME using an Agilent 7900 ICP-MS. It was used to ascertain the formulations' silver (Ag) content in a time dependent manner. The calibration curve was prepared and analyzed using AgNO3 as a blank solution. The dialysis bag method was used in this instance. Next, the time-dependent Ag ion release mechanism was evaluated in the filtered solution [17] [18].

3.12 Stability study of optimized AgNPs loaded ME formulation: The physical stability of the improved AgNPs loaded ME formulation was assessed by thermodynamic stability studies in order to tackle the problem of formulation instability during storage. The formulation underwent a 30-minute centrifugation at 3500 rpm to assess homogeneity, phase separation, and creaming, as well as thermodynamic stability. An extra stability test was then conducted, which included six cycles of heating and cooling (between 4 ^{0}C and 45^{0}C) and three cycles of freeze-thaw (between -20 ^{0}C and 25^{0}C). At least 48 hours were spent on each cycle at each temperature (Thakkar, Madan, & Lin, 2014). Throughout these trials, phase separation and colour change were seen at every temperature following each cycle. Stability tests on phase change, size, surface charge, and drug concentration were conducted for three months in a humidity chamber at 40 ± 2^{0}C and 75 ± 5% RH in compliance with ICH guidelines [19].

3.11 Inductively coupled plasma mass spectrometry (ICP-MS) analysis: This analytical technique determines the metal content and relative efficiency for AgNPs loaded ME using an Agilent 7900 ICP-MS. It was used to ascertain the formulations' silver (Ag) content in a time dependent manner. The calibration curve was prepared and analyzed using AgNO3 as a blank solution. The dialysis bag method was used in this instance. Next, the time-dependent Ag ion release mechanism was evaluated in the filtered solution.

3.12 Stability study of optimized AgNPs loaded ME formulation: The physical stability of the improved AgNPs loaded ME formulation was assessed by thermodynamic stability studies in order to tackle the problem of formulation instability during storage. The formulation underwent a 30-minute centrifugation at 3500 rpm to assess homogeneity, phase separation, and creaming, as well as thermodynamic stability. An extra stability test was then conducted, which included six cycles of heating and cooling (between 4 ^{0}C and 45^{0}C) and three cycles of freeze-thaw (between -20 ^{0}C and 25^{0}C). At least 48 hours were spent on each cycle at each temperature (Thakkar, Madan, & Lin, 2014). Throughout these trials, phase separation

and colour change were seen at every temperature following each cycle. Stability tests on phase change, size, surface charge, and drug concentration were conducted for three months in a humidity chamber at 40 ± 2^0C and 75 ± 5% RH in compliance with ICH guidelines [20].

4. RESULTS AND DISCUSSION

4.1 Pseudo-ternary plot: To determine the makeup of the region where the w/o microemulsion developed, the ternary phase diagram was made. Figure 2 (a and b) displays the highlighted portions of the ternary phase diagram for the synthesis of AgNO3 and Eribulin micro-emulsion.

The ranges of 45–70% (w/w) for oil content, 30–45% (w/w) for surfactant content, and 8–25% (w/w) for silver and reducing precursor content were chosen for the microemulsion's synthesis using a phase diagram.

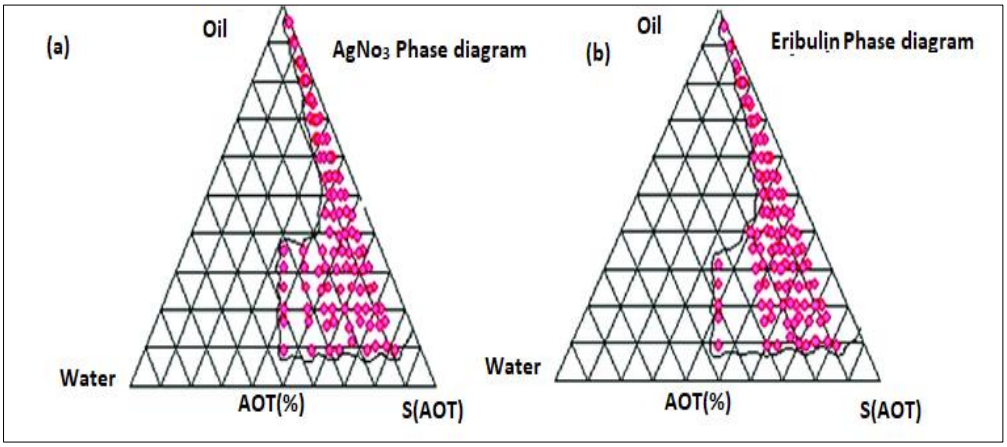

Figure 2: Pseudo-ternary phase diagram for systems of water in oil microemulsions that contain reducing agent (Eribulin) and silver precursor (AgNO3).D-Optimal mixture experimental technique

The D-optimal mixed design with 3-factor and 4-response was used to investigate and optimise the bonding between the formulation and response variables. The components of the combination cannot differ on their own since their total must equal 100% [21]. Table 6.7 lists the limits on the formulation variables. The software application Design-Expert technique 11.0.0 version was utilised to create the 12 experimental sample number matrices displayed in Table 1 and examine their correlation with the output variables. This software comprised 13 unique combinations of oil, aqueous solution, and surfactant.

Table 1: Limitations on the Proportions of Mixture Components

Designs Restrictions				
Coding of Mixture:		**Authentic**		**Miximum limit**
Lower limits (*Li*) ≤		**Restrictions (Independent variables, ≤**	***(Xi*)**	**(*Ui*)**
40.000	≤	X_1:Oil (IPM)	≤	50.000
15.000	≤	X_2:Surfactant (AOT)	≤	30.000
5.000	≤	X_3:Aqueous solution	≤	20.000
		$X_1+X_2+X_3$	=	100.000

Table 2: The D-optimal Mixture Design's twelve sample No. of experiments for optimising water-in-oil microemulsion and their outcomes values

Sample No.	Ingredient (X_1)	Ingredient (X_2)	Ingredient (X_3)	Outcome 1	Outcome 2	Outcome 3	Outcome 4
	A: Oil(IPM) %	B: Surfactantt (AOT) %	C: Aqueous solution (%)	Particle size(nm)	Viscosityy (cps)	pH	%Drug Release
1	59.00	21.00	23.00	26.00	24.20	8.15	71.00
2	61.00	26.15	15.23	38.00	32.39	6.34	75.32
3	50.01	33.10	18.20	35.21	48.00	6.22	81.22
4	56.29	25.35	20.10	13.30	57.23	6.11	82.22
5	53.60	36.00	13.11	96.12	58.00	6.12	85.00
6	48.10	31.44	23.00	72.00	51.02	6.23	82.14
7	46.00	36.00	21.00	136.01	64.00	7.42	71.00
8	61.00	22.29	19.11	24.00	23.00	7.72	69.11
9	58.01	31.38	13.32	42.44	71.22	6.02	86.00
10	55.25	30.05	17.10	4.23	68.00	6.32	86.00
11	61.00	33.00	9.00	161.21	79.00	6.18	86.21
12	51.10	28.15	23.00	26.18	41.02	6.20	86.10

4.2 Model Parameters: A particular quartic and quadratic model with a minimal predicted residual sum of square (PRESS) statistic was fitted to each of the four experimental responses using D-optimal mixing software. A minimal PRESS statistic value is frequently used to identify the best predictive model for a given collection of data [22]. A lambda value of one was required in order for the model to get better and provide the best match. Table 2 shows the values of the statistical parameters generated by the Design Expert technique for each of the four response variables. The adjusted and forecast R2 values for four answers do not differ by more than 0.01; this suggests that the model cannot account for more than 0.01% of the overall variation [23]. In the end, it evaluates the applicability of the selected models and produces a tight match between the needed model values and the actual values.

Table 3: Summary Statistics of Response Variables in the Model

Outcomes variables	Typesof model Uses	*F-stati-stic value	* Df	Prob(p value>F)	R-Squared	Adjusted R^2	Predicted R^2	PRESS
V_1(Particle size)	Special Quartic	56.20	3	0.0041	0.9996	0.9972	0.9855	441.890
V_2(Visc osity)	Special Quartic	482.8	3	0.0001	0.9999	0.9998	0.9976	16.17
V_3 (pH)	Quadratic	373.31	3	0.0001	0.9974	0.9940	0.9834	0.070
V_4(%Drug release)	Quadratic	832.66	3	0.0001	0.995	0.9970	0.9892	6.01

*Df: degree of freedom; F-value: Fischer function

4.3 Evaluation of variation (ANOVA): An analysis of the presumed mathematical model's fitness was conducted with the DOE (Design Expert) software and ANOVA. Table 3 displays the ANOVA findings for four answers. For V1 to V_4, Fischer's function, or the model F-statistics value, is 56.2, 482.8, 373.31, and 832.66, respectively, showing the applicability of the used model. The probability of receiving the F-statistics value is the p-value, according to Jeirani et al. (2012b).

The model p-values of V_1 to V_4 < 0.0001 validate the significance of the optimized model. Given that their p-values are less than 0.05, Table 6.11's quadratic coefficient terms (A^2BC, AB^2C, and ABC^2) and interaction coefficient terms (AB, AC, BC, and AC) are significant. When measured with adequate precision, the signal-to-noise ratios of V_1, V_2, V_3, and V_4 were determined to be 87.032, 233.554, 59.07, and 66.36, respectively. Table 4 lists the values of PRESS, SD, mean, and coefficient of variation (C.V.), which are clear indicators of an accurate and well-fitting model.

Table 4: The Optimized Mixture Design Model's ANOVA Table

Sum of Squares														
Outcomes	**Model**	**Linear Mixture**	**AB**	**AC**	**BC**	**A^2 B C**	**AB^2C**	**AB C^2**	**Residuals**	**Cor total**	**Std.**	**Mean**	**C.V %**	**Ad. Precision**
V_1 (Particle size)	281523.34	12884.34	3322.20	4513.44	2815.03	119.39	406.09	390.22	14.534	27816.34	3.02	56.7	4.32	87.043
V_2 (Viscosity)	3888.2	2419.42	73.89	395.98	226.44	31.96	688.20	29.18	0.24	3778.09	0.229	51.323	0.56	232.088
V_3 (pH)	6.34	3	4	0.034	0.77				0.019	6.434	0.056	6.88	0.93	59.002
V_4 (%Drug release)	489.09	138.55	340.433	13.12	2.12				0.89	491.80	0.42	80.15	0.49	66.234
***df* value**														
V_1-V_2	9	3	2	1	1	1	1	1						
V_3-V_4	6	3	2	1	1					12				
Mean Square														
V_1 (Particles size)	3532.2	6455.966	3322.12	4517.43	28.3405	119.23	4010.01	390.66						
V_2 (Viscosity)	473.09	1230.20	73.13	397.88	226.626	31.956	673.33	29.15						
V_3 (pH)	2.04	1	3	0.027	0.78									
V_4 (%Drug release)	99.01	69.77	332.24	13.12	2.823									
***F*-value**														
V_1(Particle size)	770.03	1430.89	740.42	997.06	609.65	27.23	90.89	87.69						
V_2(Viscosity)	6067.35	14996.37	946.58	5194.40	2996.53	408.16	8527.9	355.03						
V_3(pH)	358.23	328.72	993.51	9.28	260.58									
V_4(%Drug release)	689.22	484.78	2414.47	86.34	13.77									
p*-value *Prob > F														
V_1(Particle size)	<0.0001	<0.0001	0.0001	<0.0001	0.0002	0.0144	0.0026	0.0027						
V_3(pH)	<0.0001	<0.0001	<0.0001	0.0279	<0.0001									
V_4(% Drug release)	<0.0001	<0.0001	<0.0001	<0.0001	0.0119									

Positive regression coefficients indicate synergistic effects between the factor and response variables, whereas negative coefficient values in Table 4 indicate an opposing influence between the input and output variables [24]. The Design Expert analysis found that the biggest influence on the replies came from Factor C ($AgNO_3$ and eribulin precursor).

Table 5: Table of Regression Coefficients for D-Optimal Mixing Model

Coefficient Estimate									
Outcomes	**A- Oil(IPM)**	**B- Surfactant (AOT)**	**C- Aqueous solution**	**AB**	**AC**	**BC**	**A^2BC**	**AB^2C**	**ABC^2**
V_1(Particle size)	179.23	50.70	262.33	- 389.23	- 517.22	- 418.02	- 1245.22	2234.09	- 2023.00
V_2(Viscosity)	75.78	24.24	111.44	- 58.866	- 155.33	- 119.23	- 637.107	2870.23	545.23
V_3(pH)	8.18	9.51	6.41	-9.76	-0.90	-6.55			
V_4(%Drug release)	66.03	60.70	90.33	92.90	20.40	8.50			
df value									
V_1-V_2	1	1	1	1	1	1	1	1	
V_3-V_4	1	1	1	1	1	1			
Standard Error									
V_1(Particle size)	4.09	4.02	5.29	15.23	17.53	17.43	243.54	235.88	217.99
V_2(Viscosity)	0.43	0.42	0.58	2.90	3.18	3.22	32.55	31.77	29.22
V_3(pH)	0.073	0.072	0.098	0.29	0.40	0.38			
V_4(%Drug release)	0.50	0.47	0.70	1.80	2.23	2.44			
95% CI low									
V_1 (Particle-size)	169.21	41.34	245.09	- 435.23	- 570.07	- 469.40	- 2011.99	1480.11	- 2710.21
V_2 (Viscosity)	74.433	22.44	109.33	- 64.890	- 162.39	- 126.34	- 736.98	2760.89	454.32
V_3(pH)	8.00	7.43	6.23	-9.34	-1.99	-7.88			
V_4(%Drug release)	64.43	59.50	80.00	88.98	13.87	3.21			
95 % CI High									
V_1(Particle size)	177.23	61.12	283.23	- 351.43	- 465.36	- 365.32	- 473.421	2984.12	- 1328.56
V_2 (Viscocity)	7701	25.53	113.54	- 52.86	- 148.63	- 112.68	- 535.55	2968.57	636.24
V_3(pH)	8.36	9.68	6.68	-9.09	-0.15	-4.67			
V_4(%Drug release)	67.23	62.06	92.32	97.58	25.53	15.33			

To make sure that the fitting of the ANOVA parameters was fulfilled, a normal residual analysis was carried out before predicting the composition of the optimised microemulsion formulation. Figure displays a line representing the desired vs. experimental results for drug release %, viscosity, pH, and globule size. It confirms that the selected design's ANOVA parameters suit the data and offers a near match between the expected and actual responses.

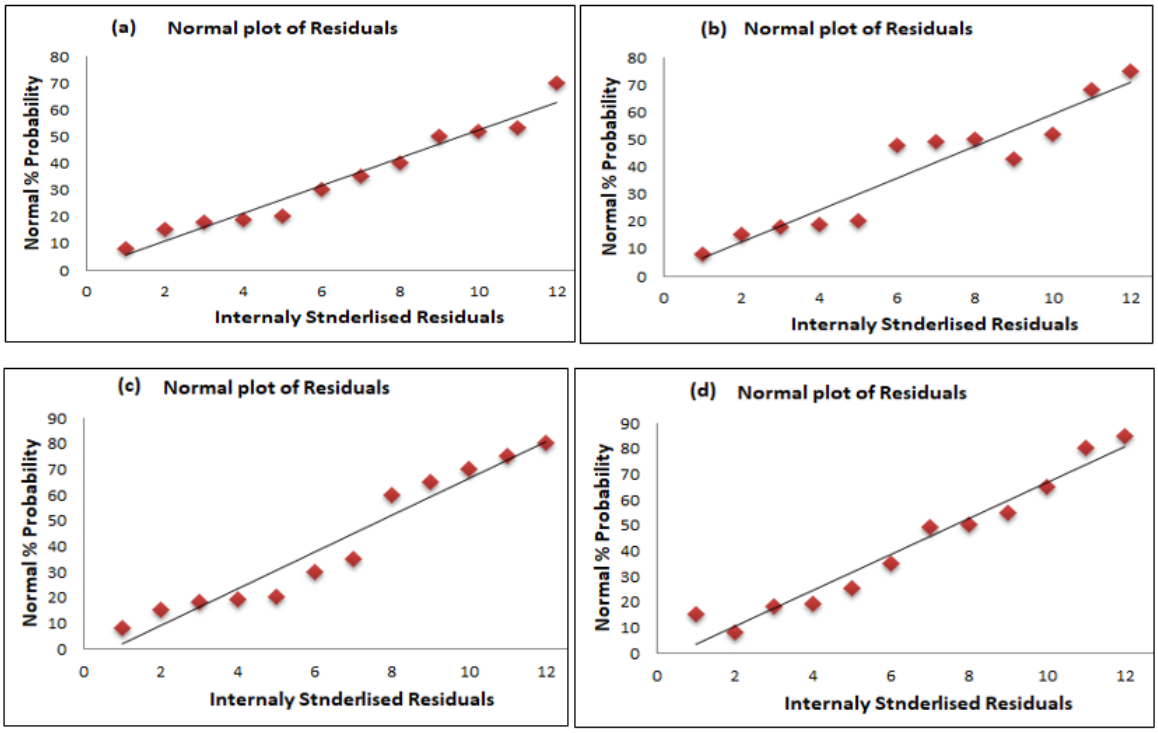

Figure 3: The line scatter graphs of model predicted versus Actual outcome, i.e.(a) Particle size, (b) Viscosity, (c) pH and (d) % Drug release from D-optimal mixturedesign

4.4 Diagnostics: Figure 4 presents the normal probability plot showing the residual analysis of the model. The points lying on the straight line indicates that the fitted model were normallydistributed with residuals and the model has been validated [25].

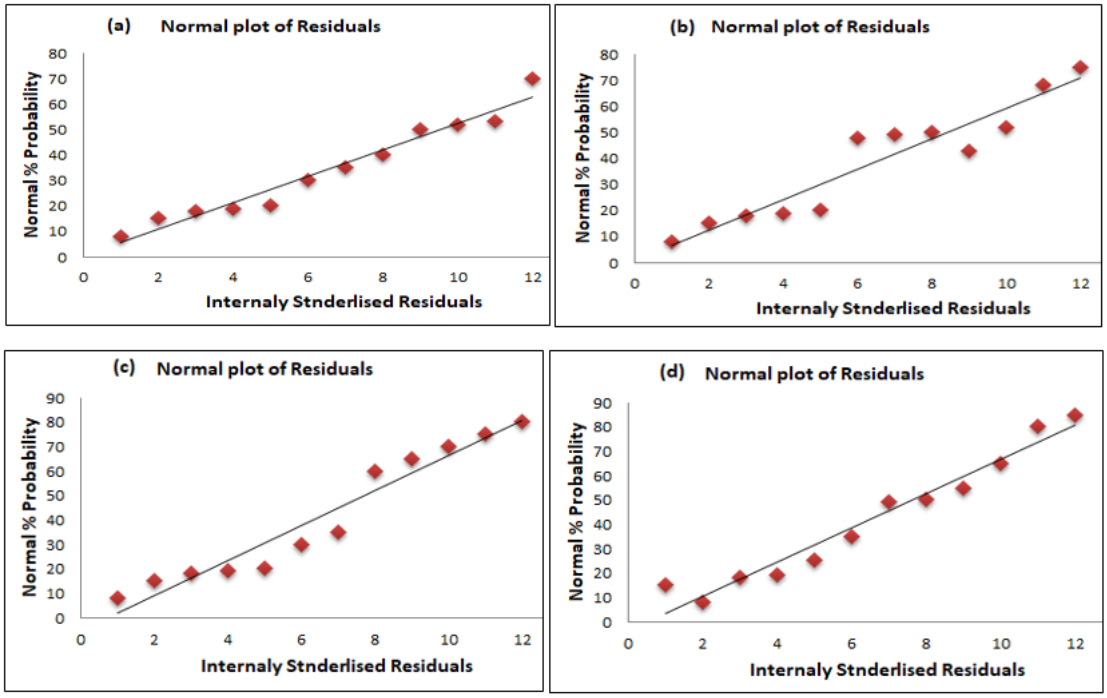

Figure 4: The typical residual plot for (a) particle size, (b) viscosity, (c) pH, and (d) percentage of drug release

The outcomes of the second diagnostic tool, the Box-Cox Plot, which validated the model, are shown in Figure 5. Four response variable Box-cox plots are shown in Figure 5 (a-d).

The optimal lambda values for globular size, viscosity, pH, and drug release are displayed using a Box-Cox plot as follows: 0.95, 1.93, and 0.40, respectively. $P < 0.05$ is shown by the red lines.

The blue line displays the value of Lambda = 1 with current transfer. In summary, the model fits the actual data rather well and satisfies the ANOVA parameter criteria.

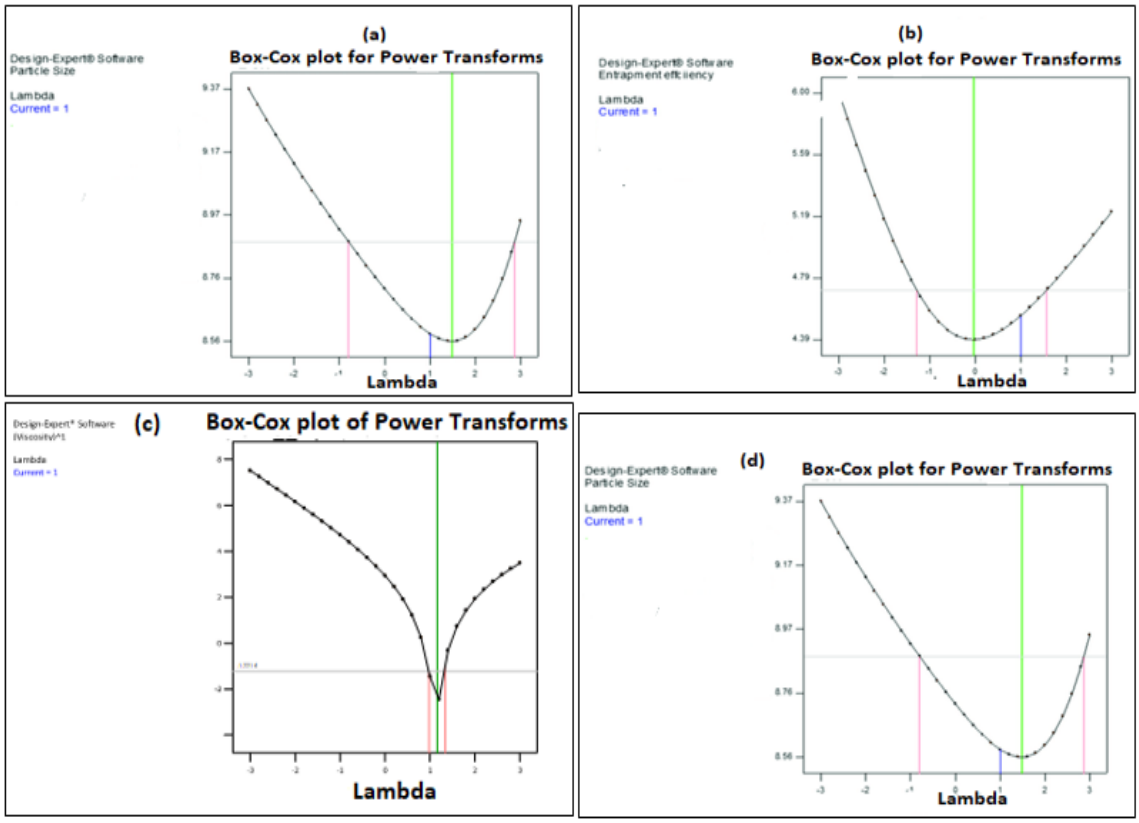

Figure 5: Box-Cox plots of (a) Particle size, (b) Viscosity, (c) pH and (d) % Drug release

4.5 Model Graphs: Figure 6 displays the contour and three-dimensional surface graphs for the Design Expert software evaluation of the effects of the formulation components on response variables.

The contour plot and surface plot of globule size (V1, Figure 6 (a and b)) indicate that decreasing the composition of water and increasing the composition of surfactant and oil led to these results [26].

Particle size was reduced and the oil/water interfacial tension was better reduced. The impact of formulation components on viscosity (V2) is seen in Figure 6 (c and d). It was discovered that the viscosity of a microemulsion increased as the oil content did.

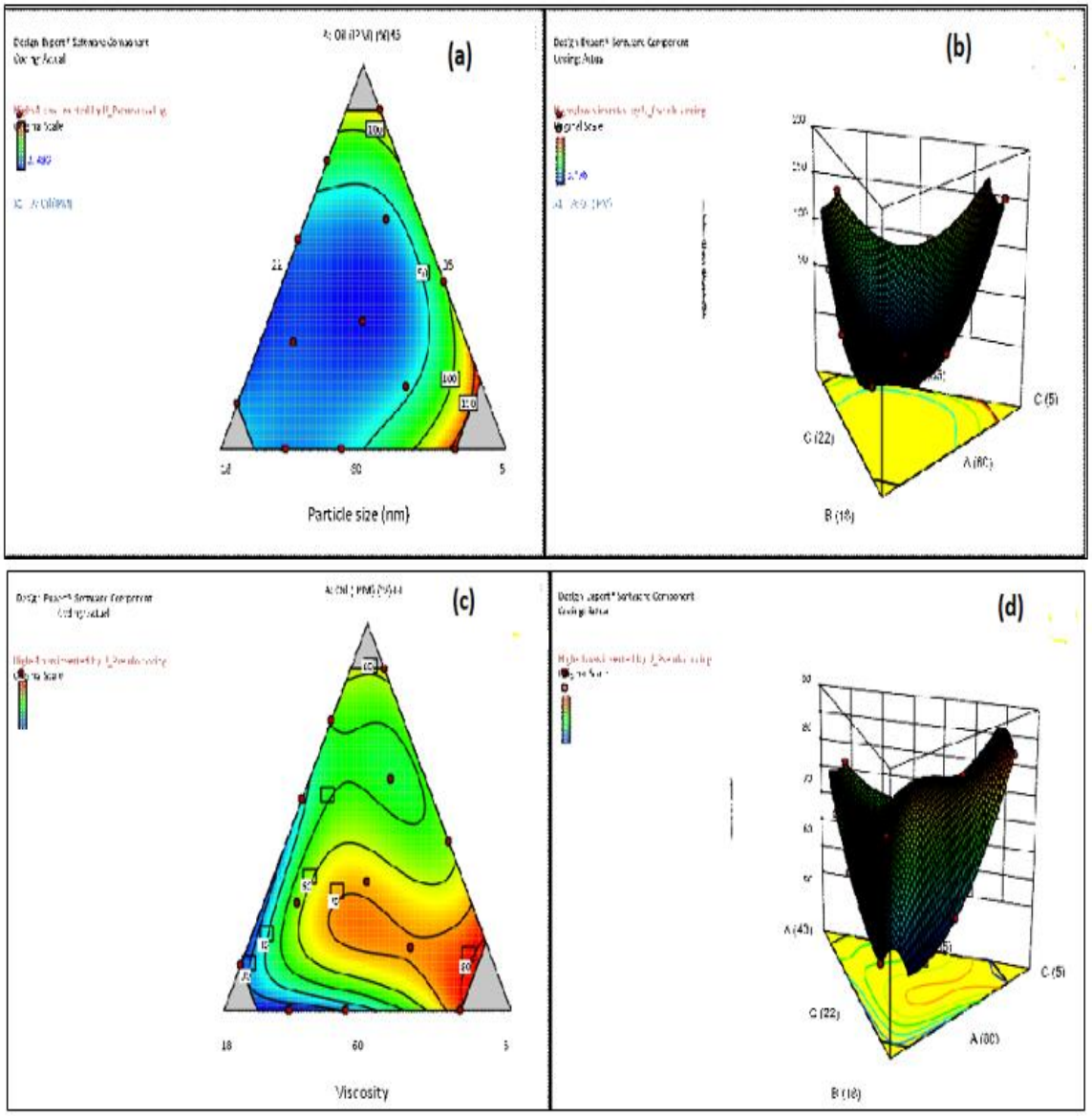

Figure 6: Plots of contours and 3-Dimensional response surface graphs that show the relationship between the responses and the formulation factors (particle size, viscosity, pH, and drug release %)

4.6 Verification of experiment model: The D-optimal Mixture Table 6 lists the expected and actual values of the output variables to evaluate the experiment model's accuracy. The model's validity was confirmed by determining that there was no significant difference between the planned and experimental values of response factors and factors, yielding a tight match to the constructed model. Response variable values for AgNPs loaded ME: Actual and Desired.

Table 6: Desired and Actual Values of Response Variables in the D-optimal Mixture Model for AgNPs-loaded ME

S. No.	V1 (Particle size)			V2 (Viscosity)			V3 (pH)			V4 (%Drug release)		
	Actual value	Predicted value	Residual	Actual value	Predict value	Residual	Actual value	Predict value	Residual	Actual value	Predicted value	Residual
1	26.00	25.53	0.38	24.50	24.38	0.12	8.46	8.33	0.03	71.00	71.02	-0.034
2	38.00	37.32	0.78	32.70	32.48	0.22	6.45	6.22	-0.034	75.70	75.70	0
3	35.40	35.66	-0.64	48.00	47.98	0.12	6.77	6.55	0	81.92	82.54	-0.74
4	13.81	14.42	-0.72	57.90	57.79	0.13	6.45	6.22	0.046	82.39	82.57	-0.19
5	96.91	97.21	-0.20	58.00	58.07	-0.072	6.95	6.97	-0.016	85.00	84.68	0.32
6	72.00	74.19	-3.40	51.30	51.98	-0.086	6.54	6.32	0.067	82.30	81.98	0.23
7	136.50	135.30	1.30	48.00	47.98	0.054	7.87	7.45	-0.014	71.00	70.84	0.069
8	24.00	24.80	-0.80	23.00	23.38	-0.30	7.56	7.32	-0.025	69.32	69.27	0.049
9	42.88	43.29	-0.64	71.92	71.80	0.12	6.13	6.13	0.02	86.00	85.86	0.26
10	4.34	3.29	0.89	68.00	68.30	-0.30	6.22	6.21	0.026	86.00	85.92	0.20
11	161.80	162.64	0.28	79.00	79.05	-0.050	6.17	6.16	0.02	86.43	86.64	-0.22
12	26.72	24.45	2.95	41.02	38.05	-3.67	6.40	6.55	-0.20	86.62	86.387	0.052

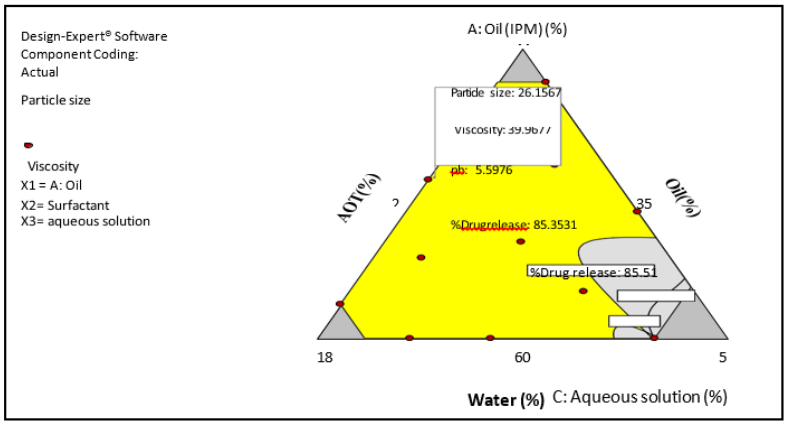

Figure 7: Plot overlaying the anticipated response values and the optimized formulation composition

The anticipated microemulsion formulation, with the size, viscosity, pH, and percentage of the particles, was represented in Figure 7 and contained 51.701% oil, 28.503% surfactant, and 22.80% water. The drug release results were found to be extremely comparable to the ideal values for Formulation No. 12 (Table 7), with values of 26.09, 40.30, 6.40, and 85.36, respectively.

Table 7: The Response Values and Composition of the Real and Model-Predicted Formulations for Optimal Formulation

Composition(%)	Predicted	Actual	Response	Predicted	Actual	RES %
Oil (IPM)	51.701	51.610	**Particle size**	26.09	26.22	2.23
Surfactant(AOT)	28.503	28.245	**Viscosity**	40.30	41.10	0.22
An aqueoussolution of (silver and Eribulin)	22.80	23.00	**pH**	6.40	6.30	1.33
			% Drug release	85.36	85.51	0.19

5. CHARACTERIZATION TECHNIQUES OF OPTIMIZED AgNPs LOADED ME:

5.1. UV-visible absorption spectral analysis: Figure 8 displays the UV-Vis spectra of ME loaded with AgNPs and Eribulin. The spectrum shows a strong plasmon absorption peak at 412 nm, which suggests that the well-dispersed AgNP synthesis in ME was performed effectively. It demonstrates how ERIBULIN's binding to silver caused a redshift in the loaded AgNPs' absorption band at 412 nm.

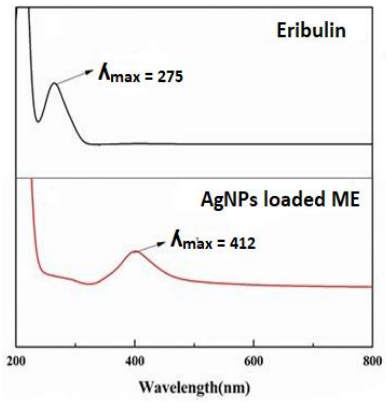

Figure 8: UV-Vis absorption peaks of the optimized AgNPs-loaded ME formulation (b) and the Eribulin formulation (a)

5.2. Globular Size and dispersity Index (PDI): The globular size of the microemulsion was found to range from 3 to 160 nm. The PDI of the microemulsion was found to be in the range of 0.2 to 0.5, which validated the monotonous distribution of the globules. The improved formulation's globular size of 25.71 with a PDI of 0.3 confirmed the uniform dispersion of particles (Figure 9).

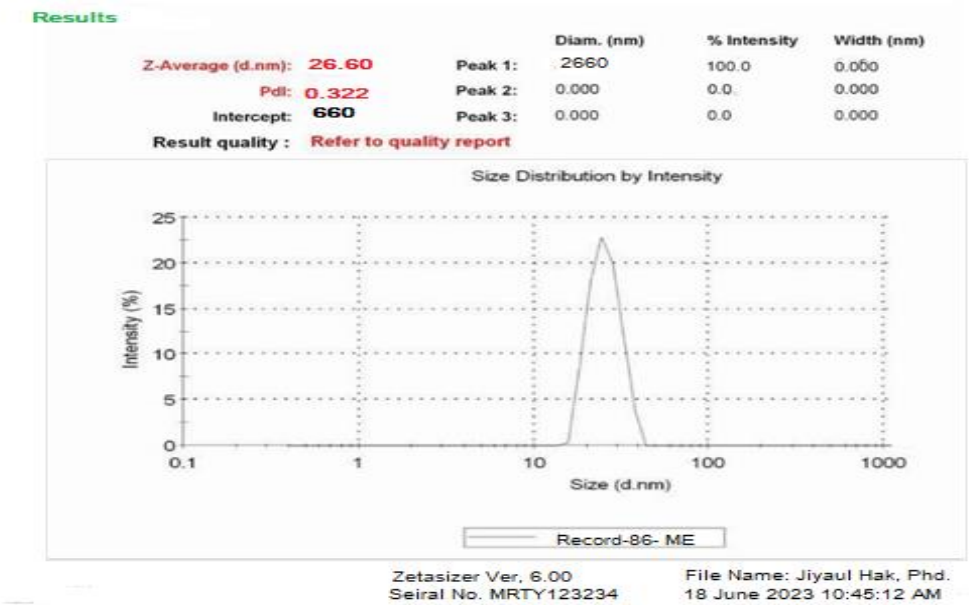

Figure 9: DLS report of the ME formulation loaded with optimized AgNPs.

5.3 Transmission electron microscopy (TEM): A size distribution histogram and TEM image are used in Figure 10 to show the morphological characteristics of the optimized microemulsion formulation. As seen in Figure 6.27, water globules with a diameter of 10–25 nm have a spherical shape. This study confirmed the spherical form and narrow size distribution of the microemulsion droplets.

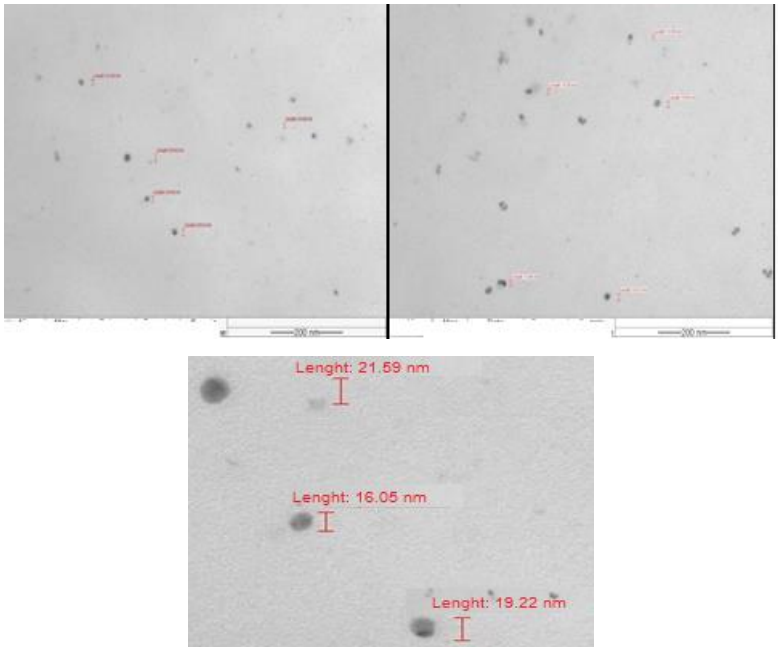

Figure 10: TEM images at lower and higher magnification of 12000 x and size distribution histogram of AgNPs loaded ME

5.5 Viscosity, pH and Conductivity: The thickness or viscosity of w/o ME was measured at 100 rpm and found to be between 22 and 70 cp. Table 6.8 shows the pH values of the formulations, which varied from 5 to 7. If consumed orally, this pH value may be within the permitted range. The pH and viscosity values of the optimised formulation were found to be 5.5±0.05 and 40.01±0.1 cp, respectively. The conductivity of the optimum formulation ease of conductive ion per unit volume is reported by R. Kumar, Kumar, and Sinha.

5.6 Density: The density of the improved formulation was found to be 0.891±0.21 g/cm3. The amount of surfactant in the microemulsion recipe will cause the formulation's density to increase. The density of the optimized formulation may pour easily and with proper flow, as indicated by the results of the density measurement.

5.7 Surface tension measurement: Surface tension measurements are employed to evaluate the stability of the AgNPs-loaded ME formulation. The surface tension of the optimized water-in-oil microemulsion was determined to be 29.8±0.057 dynes/cm. Because of its low surface tension, the formulation's thermodynamic stability and facile dispersion (micro-emulsification) are made possible by the requirement for less energy to raise the surface area, which in turn lowers the interfacial surface tension between the oil and water droplets. When surfactants are added, surface tension will drop; at a certain concentration, surface tension remains constant regardless of surfactant concentration rises. Since the water droplets in the w/o microemulsion are encircled by a continuous oil phase, the surface tension of ME is close to the oil phase, indicating the formation of water-in-oil microemulsions.

5.6 Zeta potential determination: Zeta potential study was used to evaluate the particle surface charge and the formulations' extended storage stability [27]. As seen in Figure 11, the zeta potential measurement of the optimised formulation was found to be -0.382 mV with a conductivity of 6.42 mS/cm. Because of the increased Eribulin surface charge, electrostatic energy slows down the coagulation of nanoparticles in microemulsion and maintains their stability for months. Because of their low surface charge and increased membrane permeability within the cancer cell, nanoparticles in microemulsion droplets demonstrated greater anticancer potential.

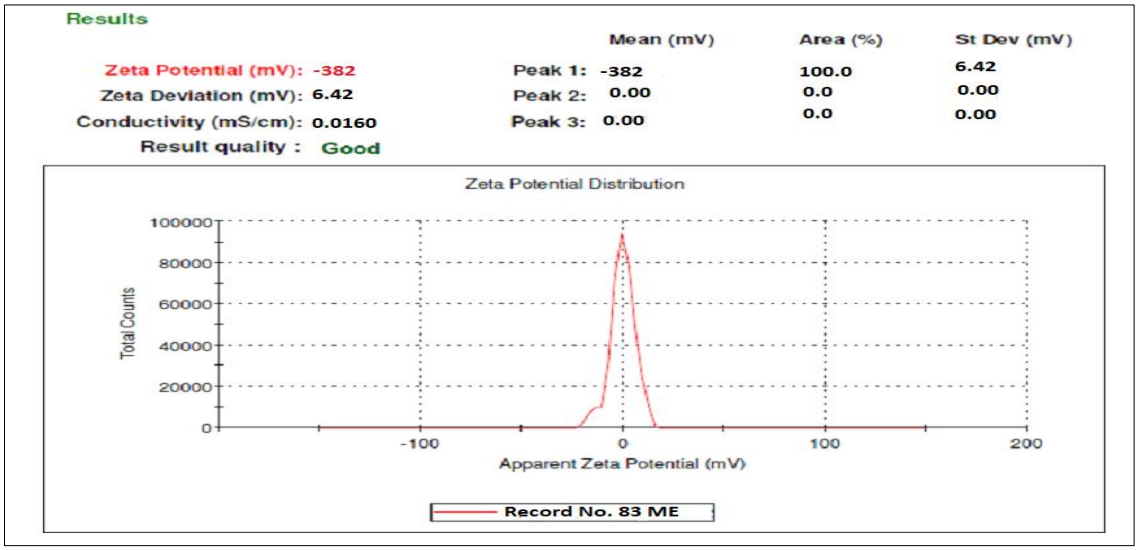

Figure 11: Zeta potential of the optimized AgNPs-loaded ME formulation represented graphically

5.7 Fourier transforms infrared (FTIR) analysis: According to Theivasanthi & AlaEribulinr, 2013b), FTIR analysis is an essential method for identifying the functional groups of AgNPs and Eribulin as well as possible atoms or molecules that control the silver ion reaction mechanism and the formation of AgNPs-loaded microemulsion. Figure 12 (a) and (b) display the FTIR spectra of the excipient combination and the Eribulin standard, respectively. The infrared spectra changed when the AgNPs-loaded microemulsion was produced (Figure 12 c). The presence of a carboxyl group in the Eribulin is confirmed by the sharp-edge peak at 1780 cm−1 and the broadband peak between 3600 and 2510 cm−1, which are caused by the stretching of the O-H (alcohol) group and a C-O vibration. This carboxyl group attaches itself to the surface of AgNPs [28].These connections completely disappeared when synthesis was finished. The absorption peak seen at 1685, 1579, and 1481 cm−1 was caused by the vibration stretch of carbon-carbon bonds in an aromatic group. The distinct peaks seen in the 1300–1000 cm−1 regions were indicative of the C–O stretch vibration and the O–H bond bending vibration of the phenolic Eribulin [29]. The presence of alcohol and phenol is indicated by the band in the 3600–2700 cm−1 band seen in Figure 12 (b), which is induced by the stretching vibration of the O–H group. According to Wang, the aromatic compounds' stretching vibration spans the C–H bond at around 3100 cm−1. The band seen in the 1300–1000 cm−1 regions of C–O and O–H bending vibration stretch vibration persisted, despite a drop in strength. Figure 12 c displays the FT-IR spectra of the AgNPs loaded ME. The C–C bond shift at 1685 and 1579 cm−1 is caused by the stretching vibration's broad band alteration at intensity 1634 cm−1, which also demonstrates that the stretching vibration's C–O bond changed from 1722 to 1634 cm−1. Figure 13 c displays the absorption band for AgNPs loaded at 3407 cm−1. ME confirms the presence of intermolecular hydrogen bonds including phenolic groups on the outside of the NPs. the shift in infrared bands caused by the interaction of the silver ions with the excipients and the creation of NPs in the microemulsion.

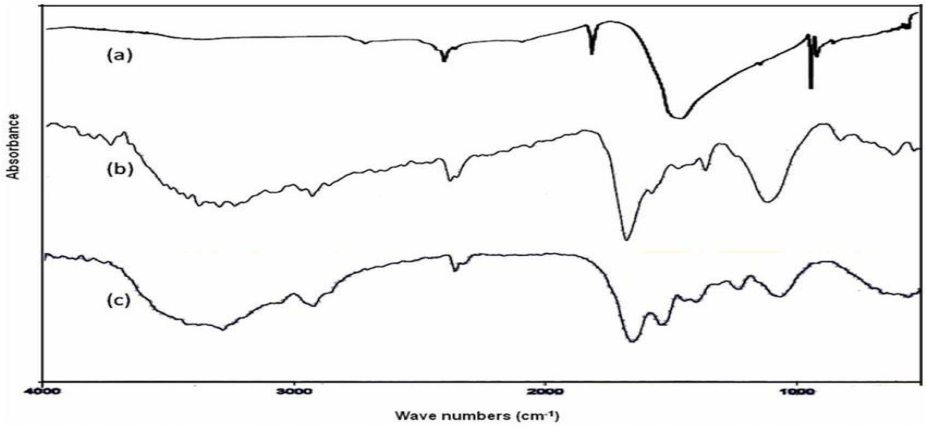

Figure 12: FTIR spectrum recorded by making KBr disc of (a) Eribulin standard (b) Excipients mixture and synthesized (c) AgNPs loaded Microemulsion

5.8 Refractive Index: The optimized AgNPs loaded microemulsions' RI of 1.43±0.01 was found to be extremely near to the oil's RI of 1.435. It verified that the w/o microemulsion was isotropic [30].

5.9 Rheological behavior measurements: The rheological analysis or flow characteristics reveal that the viscosity is quite low for all of the w/o Microemulsions. State that Newtonian flow materials with a linear connection between shear stress and shear rate are present in all formulation systems.

The rheological graph in Figure 12 (a and b) illustrates this. In conclusion, formulation techniques are appropriate for the administration of oral medications because to their low viscosity.

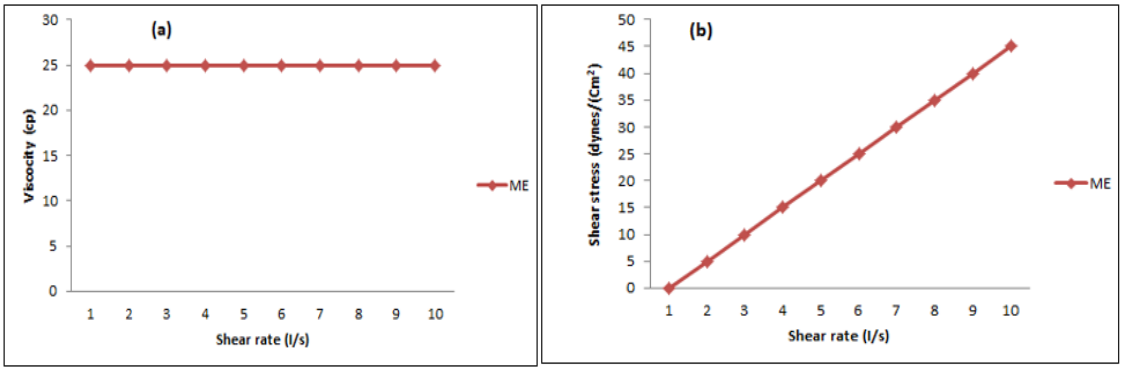

Figure 12: Linear graph of viscosity or shear rate (a) and shear stress as a function of shear rate for AgNPs loaded ME (b)

5.10 Drug content (DC) and Entrapment efficacy (EE) of Eribulin: The optimal concentration of Eribulin medication in the AgNPs loaded microemulsion was found to be 95.23±0.25% (mean± SD, n = 3). Ninety-five±0.25% was the EE percentage. It is discovered that Eribulin was uniformly distributed throughout the microemulsion and that there was very little drug loss during the formulation's manufacturing process.

5.11. Inductively coupled plasma-mass emission spectroscopy (ICP-MS): The concentration of Ag ions used for reduction by Eribulin to produce AgNPs in microemulsion was measured using ICP-MS spectroscopy. ICP-MS was used to assess the total Ag content in this solution, and the microemulsion contained 0.83 ±0.35 ppm of Ag (13), which represents 73.7% of the total Ag released from the formulation.

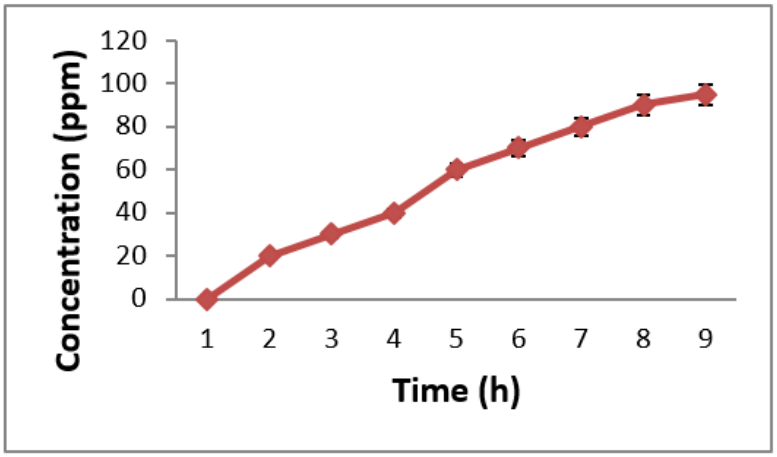

Figure 13: AgNPs loaded ME with silver detected by ICP-MS

5.12 In-vitro release study: Figure 14 displays the in-vitro release investigation of the optimised formulation. It is shown that 85.97±0.03% drug release was achieved at target cancer cell pH 5 as opposed to the systematic pH 7.4, where drug release was reported to be 69.3±0.03% during a 24-hour period. During the first step of the optimised microemulsio, the drug was released in a burst and then showed a protracted release over the course of 24 hours. It has been demonstrated that drug

release is greatest at a pH of 5, which is the pH of cancer cells, and slowest at a blood system pH of 7.4. It is concluded that the pH-sensitive properties of the produced microemulsion make it potentially useful as an effective medication delivery strategy to target cancer.

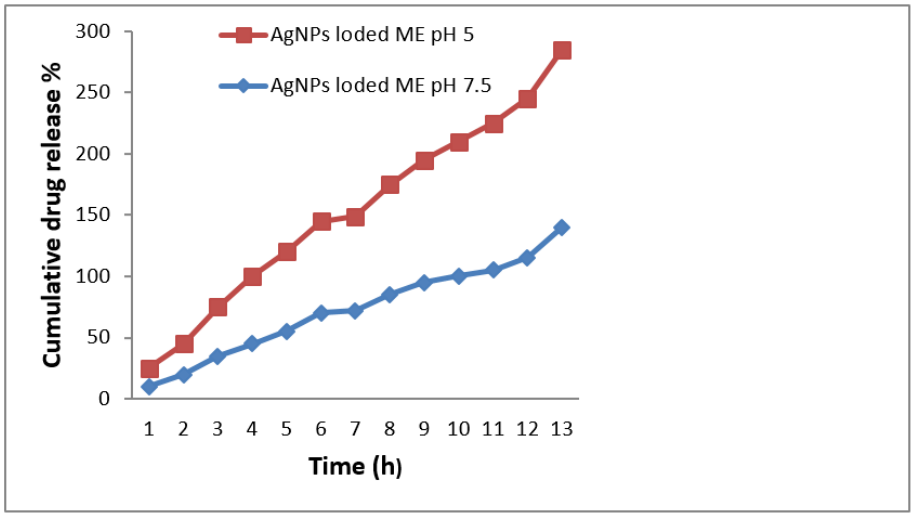

Figure 14: AgNPs loaded on the ME in vitro release graph for Eribulin at pH 5. and pH 7.4 in PBS. The results were shown as mean±SD (n=3)

5.13 Release kinetic study: The kinetic investigation (Figure 15 and Table 8) showed that the drug release from AgNPs loaded ME followed the Higuchi model at systematic pH 7.4 and cancer cell pH 5. The "n" values of 1.4 and 1.5 in the Korsmeyer-Peppas equation suggested that the drug exhibited super case II release kinetics, or controlled release behaviour. These results imply that diffusion was used to release the medicine. Drug release from such matrices can be controlled by drug diffusion, drug erosion, or both processes together.

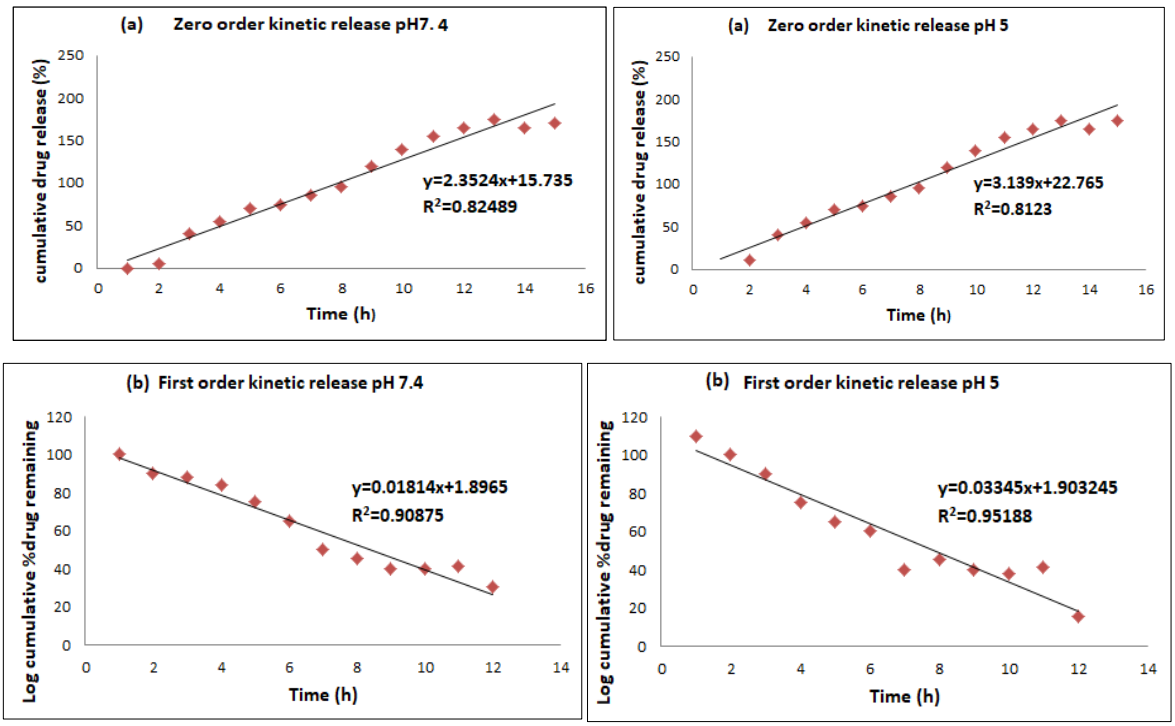

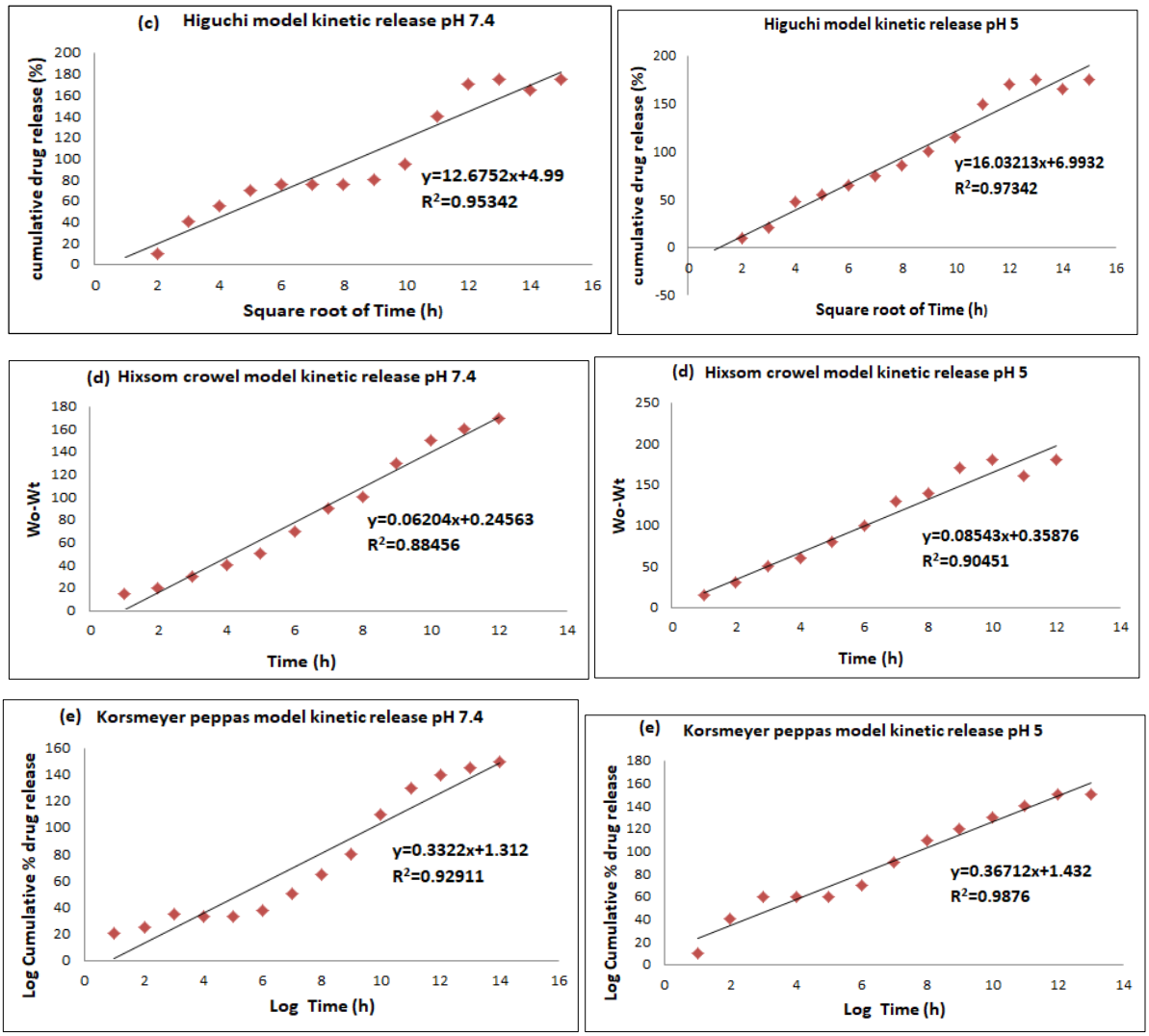

Figure 14: The drug release kinetics process of an optimised AgNPs loaded ME formulation is graphically demonstrated at (a-e) pH 7.4 and (a-e) pH 5 in the Zero, Ist, Higuchi, Hixson, and Korsmeyer-Peppas models.

Table 8: The Kinetics of Release and Their Parameters

Kinetic model	Zero-order reaction model		Ist order reaction model		Higuchireaction model		Korsmeyer -Peppas reactionmodel		Hixon crowel reaction kineticmodel	
	K	R^2	k	R^2	K	R^2	n	R^2	k	R^2
pH 7.4	3.02	0.8567	0.017	0.9123	12.15	0.9678	1.7	0.9345	0.052	0.8809
pH 5	7.12	0.9005	0.033	0.9654	18	0.9876	1.43	0.9865	0.0843	0.906

5.13 Optimized AgNP-loaded ME formulations: an antimicrobial investigation: Antimicrobial impacts of AgNPs loaded ME (1, 2, 5, 10, 15, 20, 25 and 100 µg/ml) were evaluated against Gramme+ (S. aureus), Gramme- (P. aeruginosa or E. coli), and fungal (Candida albicans) strains of bacteria. Table 6.15 displays the optimized AgNPs' ZOIs and MICs for AgNPs loaded ME formulations against E. Coli, S. aureus, P. aeruginosa, and fungus Candida albicans. The AgNPs in AgNPs loaded ME formulations demonstrated a distinct ZOI region at concentrations of 5 µg/ml and higher. The absence of a zone of inhibition in the vehicle control well demonstrated that AgNPs alone were the cause of the inhibition in bacteria and fungus. The results

show that the artificially generated in w/o microemulsion have good antibacterial activity against microorganisms. AgNPs interact with bacteria in a variety of ways that might harm them. The binding of silver nanoparticles to the surface membrane of microorganisms is the method by which they hinder the development of antimicrobials. Large surface area nanoparticles cause disruptions to the mitochondrial membrane of bacteria, interfering with their ability to function and perhaps having bactericidal effects [30].

Table 9: MICs of AgNPs-loaded ME with a Zone of Inhibition against Pathogenic Bacteria of Erbulinin Data (mean ± SD) were displayed in triplicate (n = 3)

	AgNPs loaded ME	
Bacteria's	**MIC (µg/ml)**	**ZOI (mm)**
Staphylococcusaureus	14.63±0.22	6
Escherichia coli	12.25±0.15	6
Fungus Candida Albicans	13.33±0.03	6
Pseudomonas aeruginosa	14.16±0.04	6

* MIC: Minimum inhibitory concentration; *ZOI: Zone of inhibition

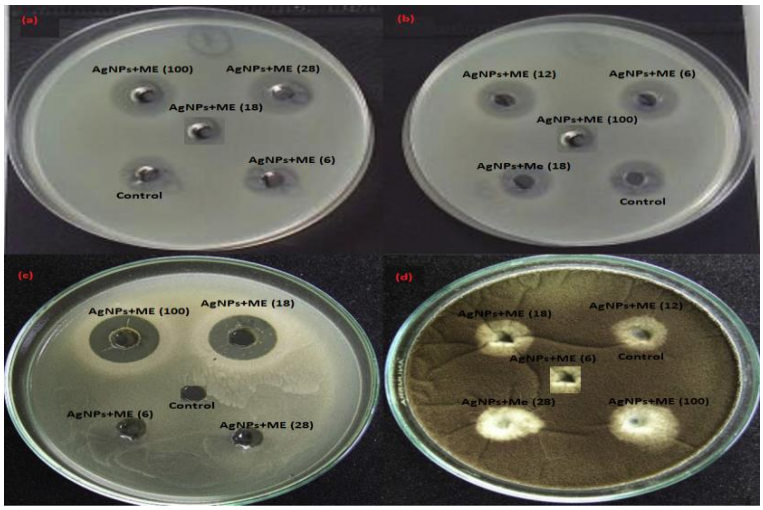

Figure 15: Antimicrobial activity of AgNPs loaded ME's different concentrations in (a) Staphylocoous aureus (b) E. coli (c) Pseudomonas aeruginosa (d) Candida albicans

5.14 Stability study of optimized AgNPs loaded ME formulation: The macroscopic analysis of the ME loaded with AgNPs revealed no phase separation or flocculation due to the Brownian movement of the microemulsion droplets. To find out how gravity affected AgNPs loaded ME, a centrifuge Eribulin investigation Eribulin was conducted. After 30 minutes of centrifugation at 3500 rpm, no phase secretion Eribulin was seen in the formulation, indicating that the particles showed excellent stability (Table 10). Three freeze-thaw cycles and six heating-cooling cycles did not exhibit phase secretion Eribulin, suggesting that the optimized AgNPs-loaded ME was thermally stable (Table 10). The AgNPs-loaded ME formulation's physical stability during a 90-day period at 40± 20%C and 75±5% relative humidity is provided in Table 10. The results of the stability test showed that the microemulsion system remained homogeneous for ninety days at 400C. The droplet size (from 26.23±1.44 to 31.98±0.69 nm) did not significantly increase throughout the course of the 90-day storage period. The Eribulin negative charge distribution of the particles showed that

the microemulsion remained stable over the storage time. Three months later, the drug concentration of AgNPs loaded ME was found to have decreased slightly from 95.88±0.34 to 92±2.44%, while the chemical composition of the formulation remained same. It is found that AgNPs-loaded ME systems exhibit good physical stability throughout the test.

Table 10: Thermal Stability Examination of AgNPs-loaded ME Formulation. The data was shown as mean ± SD for n = 3

Parameters of stability				
Centrifuge Eribulin (3500rpm)	++			
Temperature (^{0}C)	4 45	4 45	4 45	4 45
Heating cooling cycle (six cycles)	++ ++	++ ++	++ ++	++ ++
Temperature (^{0}C)	-30 35	-30 35	-30 35	-30 35
Freeze thawcycle (three cycles)	++ ++	++ ++	++ ++	++ ++

++: No phase separation

Table 11: Analysis of the Optimized AgNPs-loaded ME Formulation's Physical Stability. The data was shown as mean ± SD for n = 3

Evaluation Parameters	0 day	30th Days	60th Days	90th Days
Globule size(nm)	26.23±1.44	29.65±1.23	31.36±1.45	31.98±0.69
Zeta potential(- mV)	0.345±0.25	0.45±6.66	0.35±0.56	0.59±0.40
Drug Content (%)	95.88±0.34	94.34±0.32	94.45±0.56	92±2.44
Phase separation	No	No	No	No

6. CONCLUSION

AgNPs were synthesized using Eribulin reduction in the AOT microemulsion system in order to explore their anticancer potential an Eribulin the BC cell line (in vitro) and animal model (in vivo). Response factors impacting AgNPs generation in ME have been optimized and evaluated independently using the D-optimal mixture design and the artificial neural network model, respectively. AgNPs were demonstrated to develop in AgNPs loaded ME by physicochemical analysis. AgNPs have the uniform particle size and give the good consistency. The AgNPs loaded ME had the optimal viscosity, pH and conductivity and density. In this investigation the AgNPs loaded ME have the good zeta potential value and increase the surface charge. In this study AgNPs loaded ME have the good stability study and no change shows at various parameters. An in vitro release study confirmed that the optimized Eribulin formulation increases its bioavailability and therapeutic efficacy in targeted cancer cells as compared to healthy cells. This study also showed that AgNPs loaded into ME have the potential to be effective antibacterial agents against pathogenic bacteria and fungi. AgNPs have been demonstrated to be cytotoxic to MCF-7 cancer cell lines in AgNPs-loaded ME microemulsion, indicating that they may be employed as a possible anticancer therapy for BC. AgNPs have demonstrated a remarkable therapeutic efficacy in AgNPs loaded ME formulations that produced cancer cell apoptosis and necrosis without creating hazardous side effects to other human. This has been confirmed by both the in vivo study and the microscopic analysis. The generated AgNPs in AgNPs loaded ME formulations can be effectively used as an oral delivery vehicle for solid breast cancer.

Therefore, it is believed that AgNPs loaded into ME may be a promising anticancer therapy for solid tumors in both rodent models and cell lines.

References

1) S. Gurunathan, J. H. Park, J. W. Han, and J. H. Kim, “Comparative assessment of the apoptotic potential of silver nanoparticles synthesized by Bacillus tequilensis and Calocybe indica in MDA-MB-231 human breast cancer cells: Targeting p53 for anticancer therapy,” *Int. J. Nanomedicine*, 2015, doi: 10.2147/IJN.S83953.

2) S. Gurunathan, J. H. Park, J. W. Han, and J. H. Kim, “Comparative assessment of the apoptotic potential of silver nanoparticles synthesized by Bacillus tequilensis and Calocybe indica in MDA-MB-231 human breast cancer cells: Targeting p53 for anticancer therapy,” *Int. J. Nanomedicine*, 2015, doi: 10.2147/IJN.S83953.

3) W. R. Li, X. B. Xie, Q. S. Shi, H. Y. Zeng, Y. S. Ou-Yang, and Y. Ben Chen, “Antibacterial activity and mechanism of silver nanoparticles on Escherichia coli,” *Appl. Microbiol. Biotechnol.*, 2010, doi: 10.1007/s00253-009-2159-5.

4) P. Mukherjee *et al.*, “Fungus-Mediated Synthesis of Silver Nanoparticles and Their Immobilization in the Mycelial Matrix: A Novel Biological Approach to Nanoparticle Synthesis,” *Nano Lett.*, 2001, doi: 10.1021/nl0155274.

5) S. Chernousova and M. Epple, “Silver as antibacterial agent: Ion, nanoparticle, and metal,” *Angewandte Chemie - International Edition*. 2013. doi: 10.1002/anie.201205923.

6) Kumar, N., & Shishu. (2015b). D-optimal experimental approach for designing topical microemulsion of itraconazole: Characterization and evaluation of antifungal efficacy against a standardized Tinea pedis infection model in Wistar rats. European Journal of Pharmaceutical Sciences, 67, 97–112.

7) Wang, Y., Duan, L., Cheng, S., Chai, B., & Han, F. (2008). Water/i-Propanol/n-Butanol Microemulsions. Journal of Dispersion Science and Technology, 29(2), 280–283. https://doi.org/10.1080/01932690701707613

8) R. Preety, R. Anitha, S. Rajeshkumar, and T. Lakshmi, “Anti-diabetic activity of silver nanoparticles prepared from cumin oil using alpha amylase inhibitory assay,” *Int. J. Res.*

9) Lee, K.-S., & El-Sayed, M. A. (2006). Gold and Silver Nanoparticles in Sensing and Imaging: Sensitivity of Plasmon Response to Size, Shape, and Metal Composition. The Journal of Physical Chemistry B, 110(39), 19220–19225. https://doi.org/10.1021/jp062536y

10) Kowshik, M., Ashtaputre, S., Kharrazi, S., Vogel, W., Urban, J., Kulkarni, S. K., & Paknikar, K. M. (2003). Extracellular synthesis of silver nanoparticles by a silvertolerant yeast strain MKY3. Nanotechnology, 14(1), 95–100. https://doi.org/10.1088/0957-4484/14/1/321 Kratz, J. M., Andrighetti-Fröhner, C. R., Leal, P. C., Nunes, R. J., Yunes, R. A., Trybala, E., … Simões, C. M. O. (2008).

11) Evaluation of anti-HSV-2 activity of gallic acid and pentyl gallate. Biological & Pharmaceutical Bulletin, 31(5), 903–907.

12) Krishnaraj, C., Jagan, E. G., Rajasekar, S., Selvakumar, P., Kalaichelvan, P. T., & Mohan, N. (2010a). Synthesis of silver nanoparticles using Acalypha indica leaf extracts and its antibacterial activity against water borne pathogens. Colloids and Surfaces B: Biointerfaces, 76(1), 50–56. https://doi.org/10.1016/j.colsurfb.2009.10.008

13) Kulkarni, N., & Muddapur, U. (2014). Biosynthesis of Metal Nanoparticles: A Review. Journal of Nanotechnology, 2014, 1–8. https://doi.org/10.1155/2014/510246 Kumar, N., Dhamija, I., Vasanth Raj, P., Jayashree, B. S., Parihar, V., Manjula, S. N., … Mallikarjuna Rao, C. (2014).

14) Preliminary investigation of cytotoxic potential of 2- quinolone derivatives using in vitro and in vivo (solid tumor and liquid tumor) models of cancer. Arabian Journal of Chemistry, 7(4), 409–417. https://doi.org/10.1016/J.ARABJC.2012.12.029 Kumar, N., & Shishu. (2015a).

15) D-optimal experimental approach for designing topical microemulsion of itraconazole: Characterization and evaluation of antifungal efficacy against a standardized Tinea pedis infection model in Wistar rats. European Journal of Pharmaceutical Sciences, 67, 97–112. https://doi.org/10.1016/j.ejps.2014.10.014

16) Mandal S, Jaiswal DV, Shiva K. A review on marketed Carica papaya leaf extract (CPLE) supplements for the treatment of dengue fever with thrombocytopenia and its drawback. International Journal of Pharmaceutical Research. 2020 Jul 1;12(3).

17) Mandal S, Vishvakarma P. Nanoemulgel: A Smarter Topical Lipidic Emulsion-based Nanocarrier. Indian J of Pharmaceutical Education and Research. 2023;57(3s):s481-98.

18) Mandal S, Bhumika K, Kumar M, Hak J, Vishvakarma P, Sharma UK. A Novel Approach on Micro Sponges Drug Delivery System: Method of Preparations, Application, and its Future Prospective. Indian J of Pharmaceutical Education and Research. 2024;58(1):45-63.

19) Lehmann, B. D., Bauer, J. A., Chen, X., Sanders, M. E., Chakravarthy, A. B., Shyr, Y., & Pietenpol, J. A. (2011). Identification of human triple-negative breast cancer subtypes and preclinical models for selection of targeted therapies. Journal of Clinical Investigation, 121(7), 2750–2767. https://doi.org/10.1172/JCI45014

20) Aznar, M. Á., Lasa-Saracíbar, B., Estella-Hermoso de Mendoza, A., & Blanco-Prieto, M. J. (2013). Efficacy of edelfosine lipid nanoparticles in breast cancer cells. International Journal of Pharmaceutics, 454(2), 720–726.

21) Baker, C., Pradhan, A., Pakstis, L., Pochan, D., & Shah, S. I. (2005). Synthesis and Antibacterial Properties of Silver Nanoparticles. Journal of Nanoscience and Nanotechnology, 5(2), 244–249. https://doi.org/10.1166/jnn.2005.034

22) Wang, W., Chen, Q., Jiang, C., Yang, D., Liu, X., & Xu, S. (2007b). One-step synthesis of biocompatible gold nanoparticles using gallic acid in the presence of poly-(N-vinyl2-pyrrolidone). Colloids and Surfaces A: Physicochemical and Engineering Aspects, 301(1–3), 73–79.

23) Thapliyal, A., & Chandra, A. (2018). Antibacterial and anticancer potential of silver nanoparticles synthesized using gallic acid in bentonite/starch bio-nanocomposites. International Journal of Applied Pharmaceutics, 10(5), 178. https://doi.org//10.22159/ijap.2018v10i5.27728

24) Thapliyal, A., Khar, R. K., & Chandra, A. (2018). Artificial Neural Network Modelling of Green Synthesised Silver Nanoparticles in Bentonite/Starch Bio-Nanocomposite. Current Nanoscience, 14(3), 239–251.

25) Theivasanthi, T., & Alagar, M. (2013a). Konjac Biomolecules Assisted–Rod/Spherical Shaped Lead Nano Powder Synthesized by Electrolytic Process and Its Characterization Studies. Nano Biomedicine and Engineering, 5(1). https://doi.org/10.5101/nbe.v5i1.p11-19

26) Sophia V. Kyriacou, William J. Brownlow, and, & Xu*, X.-H. N. (2003). Using Nanoparticle Optics Assay for Direct Observation of the Function of Antimicrobial Agents in Single Live Bacterial Cells†. https://doi.org/10.1021/BI0351110 Sotiriou, C., & Pusztai, L. (2009).

27) Gene-Expression Signatures in Breast Cancer. New England Journal of Medicine, 360(8), 790–800.

28) Soule, H. D., Vazguez, J., Long, A., Albert, S., & Brennan, M. (1973a). A human cell line from a pleural effusion derived from a breast carcinoma. Journal of the National Cancer Institute, 51(5), 1409–1416.

29) Retrieved from http://www.ncbi.nlm.nih.gov/pubmed/4357757 Soule, H. D., Vazguez, J., Long, A., Albert, S., & Brennan, M. (1973b).

30) A human cell line from a pleural effusion derived from a breast carcinoma. Journal of the National Cancer Institute, 51(5), 1409–1416.

31) Retrieved from http://www.ncbi.nlm.nih.gov/pubmed/4357757 Sparano, J. A., & Solin, L. J. (2010). Defining the Clinical Utility of Gene Expression Assays in Breast Cancer: The Intersection of Science and Art in Clinical Decision Making. Journal of Clinical Oncology, 28(10), 1625–1627.